INTERFACE

royalsocietypublishing.org/journal/rsif



Review

**Cite this article:** Sharp AJ, Betts TR, Banerjee A. 2026 Statistical shape modeling in cardiovascular disease: a narrative review. *J. R. Soc. Interface* **23**: 20250785.
https://doi.org/10.1098/rsif.2025.0785

Received: 29 July 2025
Accepted: 19 December 2025

**Subject Category:**
Life Sciences–Engineering interface

**Subject Areas:**
biomedical engineering, computational biology

**Keywords:**
statistical shape modeling, point distribution model, principal component analysis, cardiovascular disease, heart

**Author for correspondence:**
Abhirup Banerjee
e-mails: abhirup.banerjee@eng.ox.ac.uk; abhirup.banerjee88@gmail.com

THE ROYAL SOCIETY PUBLISHING

# Statistical shape modeling in cardiovascular disease: a narrative review

Alexander James Sharp[1,2], Timothy R. Betts[2] and Abhirup Banerjee[1]

[1]Department of Engineering Science, University of Oxford, Oxford, Oxfordshire, UK
[2]Cardiology Department, Oxford University Hospitals NHS Foundation Trust, Oxford, UK

AJS, 0000-0002-5994-7798; TRB, 0000-0001-9063-9905; AB, 0000-0001-8198-5128

Cardiovascular diseases (CVDs) remain a leading cause of mortality worldwide. We explore the application of statistical shape modeling (SSM) as a powerful tool in cardiac anatomy assessment, facilitating innovative approaches to diagnosis and treatment. SSM uses advanced mathematical and statistical techniques to understand the geometric properties of anatomical structures across populations. By identifying significant shape parameters, it captures and quantifies subtle variations that may elude traditional approaches. We discuss its evolution, from landmark-based methods to point distribution models for establishing the point-to-point correspondence crucial for accurate shape analysis. We delve into the statistical techniques used to measure shape variability, with a focus on principal component analysis for dimensionality reduction. Key evaluation metrics in the assessment of model performance, such as compactness, generalization and specificity, are reviewed. The clinical utility of SSM across the spectrum of CVDs is examined, covering diagnosis, risk stratification, treatment optimization, follow-up and research applications. Future directions, including the development of multi-label models, integration of deep learning approaches, and spatio-temporal SSM to capture dynamic changes in cardiac geometry, are considered. Through this narrative review, we aim to underscore SSM's promise as a powerful tool in combating CVDs and advancing personalized medicine, ultimately improving patient outcomes.

## 1. Introduction

Cardiovascular diseases (CVDs) stand as one of the most pressing health challenges of our time, exerting a profound impact on global health and healthcare systems. They are the leading cause of death globally, claiming in excess of 19 million lives annually, this figure representing approximately one-third of all deaths [1]. The prevalence of CVDs is not merely a health concern but also an economic one; within the European Union, the direct and indirect costs associated with CVD are estimated at €282 billion [2]. This economic burden, coupled with the immense human cost, underscores the urgent need to enhance understanding, diagnosis and treatment of CVDs through innovative approaches.

In response to this challenge, the medical community has increasingly turned to advanced imaging and computational methods. Leveraging advances in three-dimensional imaging techniques that can produce anatomically accurate reconstructions of structures, statistical shape modeling (SSM) has emerged as a particularly promising tool in the field of cardiac anatomy assessment [3]. SSM is a computational process that applies mathematics, statistics and computing to analyze and represent the geometric properties of anatomical structures across a population [4]; through the identification of significant shape parameters, both average shape and shape variability can be described in a compact, quantitative format [5,6].

Using such a mathematical framework to represent anatomical structures, SSM enables testing of biologically relevant hypotheses through population-level analysis of shape variations [7]. Such applications build upon the principle that the shape of anatomical structures contains valuable information about their function and potential pathologies. In the context of cardiac anatomy, the heart's shape is intimately linked to its function, and subtle variations in geometry can be indicative of underlying disease processes or predictive of future cardiac events. SSM provides a means to capture these subtle variations in a quantitative and statistically rigorous manner, offering insights that may not be apparent through traditional visual inspection of medical images.

This narrative review aims to elucidate the current state of SSM in cardiac assessment, exploring its technical foundations and potential to address pressing challenges in CVD. We will examine several key aspects:

(1) *Representation of three-dimensional geometry*. A critical aspect of SSM is how three-dimensional cardiac geometry is represented mathematically. We will discuss the evolution of landmark approaches through to the latest point distribution models (PDMs), in particular, highlighting methods for establishing point-to-point correspondence between different geometries in a population. While PDM-based methods form the core of this review, deformation-field approaches will also be briefly described.
(2) *Three-dimensional shape analysis*. At the heart of SSM is the application of statistical techniques to analyze shape variability. We will focus on principal component analysis (PCA), the most commonly used method in SSM, explaining its mathematical basis and how it is applied to extract principal modes of shape variation in populations.
(3) *Evaluation metrics and validation*. Evaluating the performance and accuracy of models is crucial for their application in clinical and research settings. We will discuss the key evaluation metrics of compactness, generalization and specificity, as well as task-level validation.
(4) *Clinical applications*. The true value of SSM lies in its clinical applications. We will explore how SSM is being used in various aspects of cardiovascular medicine, including diagnosis, treatment and research. To ensure broad coverage of the field and to highlight the diverse ways in which SSM techniques are being translated into clinical practice, this section includes studies using both PDM and deformation-field-based approaches.
(5) *Challenges and future directions*. While SSM has shown great promise in cardiac assessment, there are several challenges and emerging areas of research that warrant attention. We will discuss barriers to clinical uptake, the importance of moving beyond single-structure models to capture the heart's complex, interconnected nature, examine how deep learning approaches are addressing the limitations of traditional SSM techniques, and explore the potential of spatio-temporal SSM to provide a more complete understanding of cardiac shape and function over time.

Through this comprehensive examination, we hope to demonstrate SSM's potential as a powerful tool in combating CVD.

## 2. Sources and selection

To identify relevant studies, we conducted targeted, non-systematic searches of Ovid MEDLINE, Embase and IEEE Xplore (last searched: 26 May 2025). These databases were selected to ensure coverage across both clinical and engineering domains. The searches combined terms related to SSM (e.g. 'statistical shape model*', 'shape analysis') with cardiac-related anatomical (e.g. 'heart', 'cardiac', 'ventricle') and pathological terms (e.g. 'coronary artery disease', 'cardiomyopathy', 'atrial fibrillation'). Searches were restricted to titles and abstracts to maintain focus on relevant content. Additional references were identified through manual screening of bibliographies from included studies and recent reviews. Selection was purposive, with studies chosen to illustrate methodological variants and clinically oriented applications.

## 3. Representation of three-dimensional geometry

### 3.1. The evolution of point distribution models

Traditional geometric morphometrics capture and compare geometries within a population using the coordinates of landmarks placed on the two- or three-dimensional surface [8,9]. Depending on the field of study, the locations of these landmarks can have different nomenclature. Commonly, three types are described [10,11]: anatomical landmarks at points of biological significance, or points of application-dependent significance; mathematical landmarks at points of geometric significance, or points of application-independent significance; and pseudo-landmarks that are points interpolated from the previous two types, for example, points equally spaced around a shape outline between two anatomical landmarks.

Manual identification of such landmarks has important limitations, being expert driven, subjective and time consuming [7]. Furthermore, resultant models are sparse, with the limited number of landmarks unsuitable for comparing complex three-dimensional anatomies [12]. PDMs are the computational extension of morphometric landmark approaches; dense sets of hundreds or thousands of points are produced automatically to model geometry with greater fidelity and without observer bias [10,13] (figure 1*a*). As with landmarks, these points are placed at comparable locations between geometries within the population, and as such are known as correspondence points [14] (figure 1*b*). As their position cannot be determined manually, their appropriate location must be extrapolated from the shapes themselves [15].

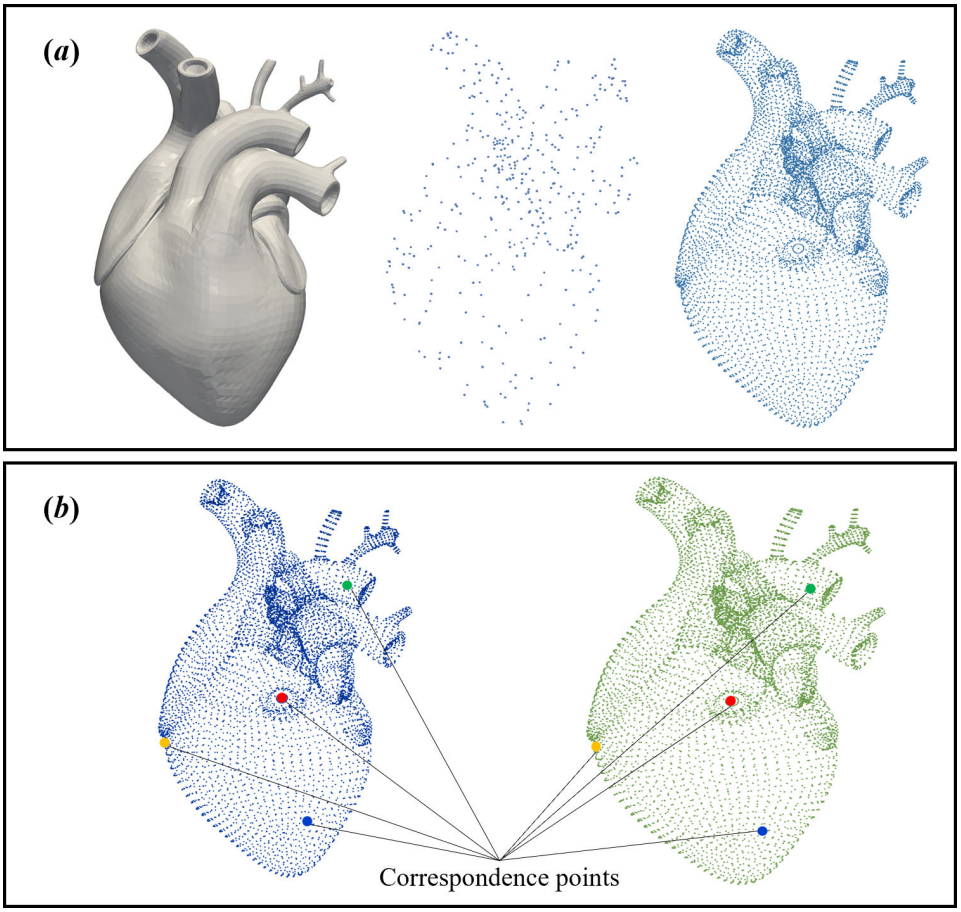


**Figure 1.** Point distribution models. (*a*) While a limited number of points can adequately represent simple geometries, complex three-dimensional anatomies require dense sets of points. Here, we depict three representations of the same heart surface: (left) polygonal surface mesh; (middle) sparse landmarks (example of under-sampling for complex anatomy); (right) dense point distribution model. (*b*) Statistical shape modeling requires point-to-point correspondence, such that their locations can be compared between similar geometries within a population.

## 3.2. Correspondence in point distribution models

Computation of correspondence points is generally posed as an optimization problem, where an objective function is defined and minimized [16]. Approaches can be categorized as pairwise or groupwise: the former treats each geometry within a population individually; the latter considers variability across the entire population of geometries to establish correspondence points simultaneously [7,17].

### 3.2.1. Pairwise approaches

Pairwise methods seek to establish correspondence points through the use of a template geometry [17]. At its simplest, this may take the form of choosing one geometry within a population to be a template. This template geometry, along with the other geometries within the population, is manually annotated with a sparse number of anatomical landmarks. These landmarks are then used to register and deform the template geometry to each of the other cases and to extend the sparse correspondence [3,4,18]. Such an approach reduces the computational complexity of producing dense correspondences; however, it remains expert-driven, time-consuming and resultant models have a bias towards the template geometry [7,16].

Alternatively, parameters based on fixed geometrical bases can be used to establish correspondence. Geometries are represented by these parameters in a standard parameter space, with correspondence established between points with the same parameter space coordinates [4,17]. Spherical harmonics point distribution model (SPHARM-PDM) [19] is an open-source software tool that uses such a parametric method. A sphere acts as the template by providing a standardized parameter space, with spherical harmonics used to describe individual geometries parametrized onto this sphere. The optimization problem involves computing spherical parametrizations through an equal area mapping of individual geometries to the sphere while minimizing angular distortions. The spherical harmonic basis function is denoted as $Y_l^m(\theta,\phi)$, where $l$ is the degree, $m$ is the order, $\theta$ is the polar angle and $\phi$ is the azimuthal angle. This is defined as

$$Y_l^m(\theta,\phi) = \sqrt{\frac{2l+1}{4\pi}\frac{(l-m)!}{(l+m)!}}P_l^m(\cos\theta)e^{im\phi}, \tag{3.1}$$

where $P_l^m$ are the associated Legendre polynomials.

Each geometry is represented by a SPHARM description, which consists of a set of coefficients that weight the spherical harmonics. Correspondence is established by aligning the first-order ellipsoids of individual geometries spherical harmonic

coefficients to the axes of the basis functions. Following this normalization, points on the geometries that share the same parametrization are considered correspondence points. A specific limitation of SPHARM-PDM is the requirement for geometries with spherical topology. A fundamental limitation of all pairwise methods is their inability to incorporate population-wide variability in the optimization process [4].

### 3.2.2. Groupwise approaches

Groupwise approaches optimize correspondence points for all geometries in a population simultaneously, enabling them to capture additional population-specific metrics within the optimization that pairwise approaches are unable to [3]. This is particularly advantageous in populations with greater variability in geometry between individuals, as it does not penalize this natural variation [7].

ShapeWorks [20] is an open-source software tool that uses a groupwise approach called particle-based shape modeling (PSM). PSM is in an entropy-based optimization, which is non-parametrized and therefore independent of topology, can handle open surfaces, and does not require an initial template. Following initialization with a single particle on each geometry, an iterative approach of particle-splitting and correspondence optimization is used, until the system is optimized for the user-specified number of particles. The number of particles is determined by balancing the need for accurate geometric representation, geometric complexity within the population, and computational resources.

Correspondence optimization is achieved by minimizing an energy function ($Q$), defined by

$$Q = H(Z) - \sum_{k=1}^{N} H(X_k)\,. \tag{3.2}$$

The first term is a shape space (discussed further in §4.1.) variable, which considers how the correspondence points on the surfaces of all geometries within a population are positioned. $Z$ represents the distribution of shapes in the shape space, with entropy ($H$) estimated assuming Gaussian shape distribution in shape space. Minimization of this variable equates to a more compact model.

The second term is a particle distribution variable, which considers how particles are positioned on the surface of each geometry. $X_k$ represents the distribution of particles on the $k$th shape. Entropy is estimated based on Euclidean particle-to-particle repulsion, and maximization of this variable equates to more accurate geometric representations through uniform distribution of particles on the surface.

Alignment of geometries is a key consideration, with clear implications for the shape space variable. In the absence of pre-existing information on correct alignment, this may first be performed based on geometries' centres of mass or by an iterative closest point algorithm. Subsequently, during the optimization, alignment may be refined using generalized Procrustes analysis (GPA) (discussed further in §4.1.) once all particles have been initialized.

## 3.3. Deformation-field-based approaches

Deformation-field-based approaches to SSM offer an alternative to point-based methods, such as PDMs, for establishing anatomical correspondence across a population. In these approaches, correspondence is established implicitly through non-rigid registration, wherein each subject's geometry is aligned to a common template by estimating a dense deformation field that warps the template to match the target shape. This deformation field is assumed to encode the geometric transformation required to align anatomical structures and is treated as a proxy for establishing correspondence between subjects. The underlying assumption is that homologous anatomical points across individuals will map to the same location in the template space once registration is complete [7,21]. Once deformation fields have been computed for a cohort, statistical techniques are applied to the deformation parameters (e.g. displacement vectors or transformation coefficients) to analyze population-level shape variation.

The anatomical fidelity of correspondences inferred from deformation fields depends on the registration algorithm and the similarity metrics used to guide alignment. Different approaches adopt different registration formulations, and even on the same data, different algorithms can yield measurably different mappings [22]. The choice of template can also bias results, although groupwise template-building strategies mitigate this effect [7].

At the same time, deformation-field approaches offer important strengths. They provide dense, spatially smooth representations, do not require predefined landmarks, and naturally support atlas construction [23]. They are particularly attractive when point-to-point homology is ambiguous, for example, in structures such as the aorta, whose long, quasi-cylindrical, largely featureless wall, and variable branch take-off positions create circumferential and longitudinal ambiguity in point matching; small rotations or shifts along the centreline yield equally plausible correspondences, making landmark-based homology ill-posed. In such settings, population statistics computed on deformation parameters and visualizations of displacement fields can reveal clinically interpretable patterns [24–27].

Although PDMs remain the focus of this review, for further technical details of deformation-field-based modeling, readers are referred to the open-source software tool Deformetrica [23]. Additional examples of clinical applications are also discussed in §6.

# 4. Three-dimensional shape analysis

## 4.1. Shape alignment

Shape can be defined as the geometric information describing an object independent of its pose [28]. In a PDM, correspondence points are represented as coordinates in a high-dimensional configuration space. To focus solely on shape variation, we need to remove similarity transformations (translation, scale and alignment) from these correspondence point configurations, transitioning from configuration space to Kendall's shape space [3,29]. This is commonly achieved through GPA [20,30], using the GPA algorithm of Gower [31], modified by Ten Berge [32].

GPA is an extension of ordinary Procrustes analysis, with the key difference being its ability to align multiple shapes simultaneously by way of an iterative alignment process towards a computed mean shape that best represents all geometries in the dataset [33]. In the context of correspondence points, configurations are first translated such that their centroids (mean of all points) align with an origin. They are then scaled to a common size by dividing each coordinate by the root mean square distance of all points from the centroid. An initial alignment is performed, choosing one configuration as a reference. A mean configuration is then calculated by averaging the correspondence points across all configurations following this initial alignment. This mean shape is then used and recalculated in an iterative alignment process to minimize the mean squared distance between configurations [8]. Statistical analyzes can subsequently be performed in this Procrustes space, as measured distances are good linear approximations of geodesic distances in shape space [20].

## 4.2. Variability between shapes

Following superimposition of a population of correspondence points, using GPA or otherwise, a mean geometry can be defined by computing the averages of correspondence point positions [34]. Such a pointwise analysis can also be used to determine local geometric variability, with hypothesis tests applied to visualize regions of significant difference between groups; however, such an approach requires false detection correction due to the number of correspondence points tested, reducing the statistical power of such analysis [35].

Analysing high-dimensional PDM data in the full shape space, which combines all correspondence points (figure 2*a*), can help avoid issues with multiple comparisons. However, this approach presents its own challenges as traditional statistical methods are not suitable for such high-dimensional spaces; as the number of dimensions increases, estimators converge to the true parameter values much slower in relation to the sample size, and as such, the amount of data required for accurate parameter estimation is prohibitive [35]. In addressing this challenge, PCA has become the primary technique for dimensionality reduction in PDMs, facilitating subsequent conventional multivariate analysis.

### 4.2.1. Principal component analysis

PCA is a powerful multivariate statistical method that reduces the dimensionality of large datasets while preserving their essential information content [36,37]. It achieves this by creating new variables called principal components (PCs), which are linear combinations of the original variables. These PCs are orthogonal and arranged in order of decreasing variance, with the first PC capturing the maximum possible variance, the second PC capturing the maximum remaining variance and so on. This approach allows for the identification and retention of significant information while discarding less important components. The foundation of PCA lies in the analysis of covariance between variables and the subsequent eigenvalue decomposition of the covariance matrix. Eigenvectors derived from this process define the directions of the new PC axes in multidimensional space, with their corresponding eigenvalues indicating the amount of variance explained by each PC.

While PCA is widely used, it faces two key challenges in shape analysis: determining the optimal number of PCs to retain and effectively visualizing group differences [35]. The first challenge, known as the factor analysis problem, can significantly impact statistical results depending on the number of PCs chosen. Various methodologies have been developed to address this issue. These range from simple conventions, such as retaining only PCs that account for a percentage of total variance, to more sophisticated approaches like parallel analysis. Parallel analysis [38] aims to identify components with variance distinguishable from noise, modelled as an isotropic, multivariate unit Gaussian; this approach helps differentiate between meaningful variation and noise, which in the context of PDMs may result from image sampling.

The second challenge of visualization is crucial in relating statistical test outcomes to scientific hypotheses. One approach is to transform group differences observed in the reduced-dimensional PCA space back to the original, full-dimensional shape space; once transformed, these differences can be visually represented as deformations on the mean geometry (figure 2*b*). Alternatively, the mean geometries of each group can be visualized and compared.

A further practical consideration is whether to normalize for overall scale during alignment, and this should be reported clearly, as it materially alters the covariance matrix and the estimated PCs. As previously discussed, full Procrustes alignment rescales each instance to unit centroid size. Rescaling removes non-shape variation so that the covariance structure, and thus the PCs, reflect shape differences alone. This can be advantageous as it prevents overall size from dominating the decomposition and overshadowing subtler, local deformations. Conversely, in datasets exhibiting allometry (systematic coupling between size and shape), enforcing equal scale can obscure biologically relevant trends, and partial Procrustes that preserves scale may be more appropriate.

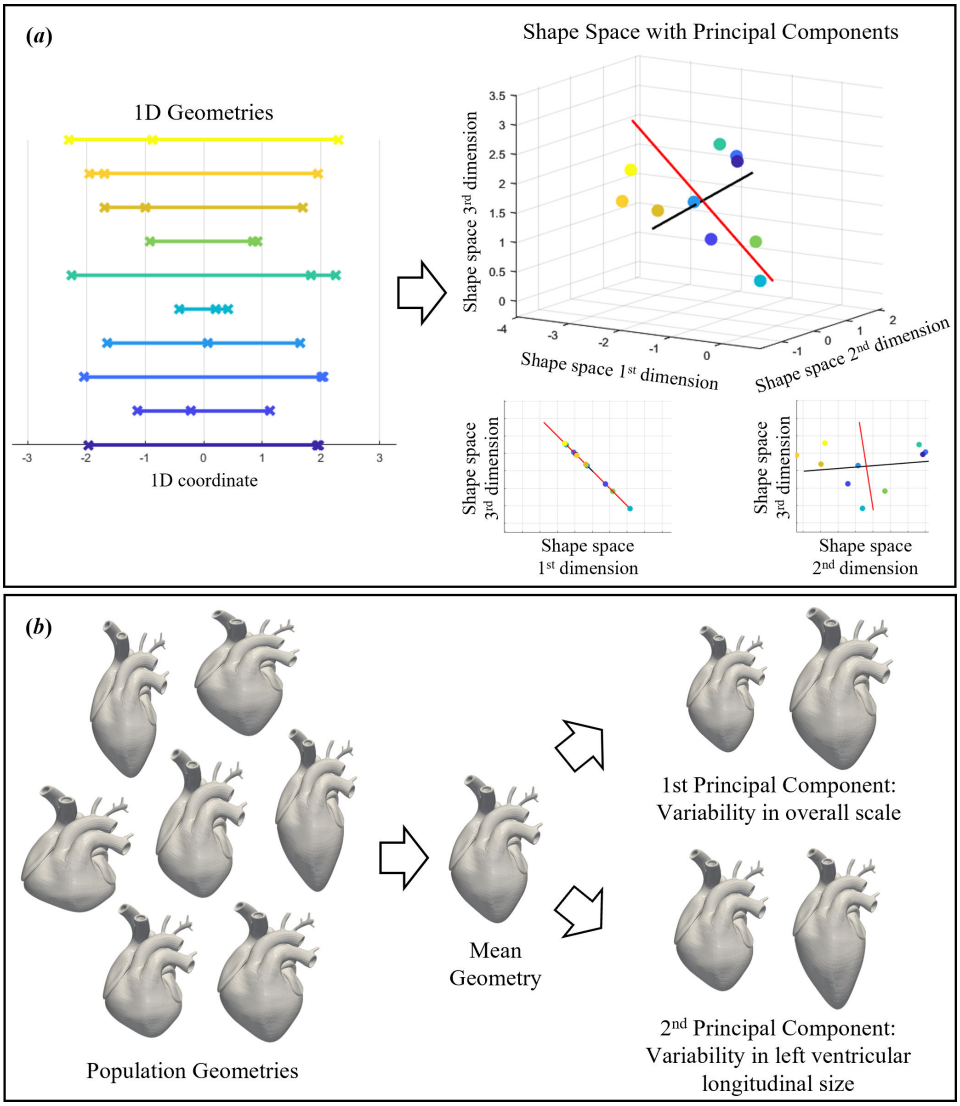


**Figure 2.** Principal component analysis applied to statistical shape modeling. The correspondence points that describe a geometry can be represented as a single point in multidimensional shape space. (*a*) A population of one-dimensional shapes, each with three correspondence points (crosses), is visualized in a three-dimensional shape space, with PCA reducing dimensionality along two principal components (red and black lines). (*b*) For three-dimensional geometries, PCA captures major modes of shape variability, visualized by deforming the mean geometry along principal component modes.

By effectively addressing these challenges, PCA enables the creation of PDMs that encode the probability of geometry occurrences in terms of a mean and a hierarchy of major modes of variation, ultimately facilitating improved interpretation and visualization of complex datasets.

## 5. Evaluation metrics and validation

### 5.1. Extrinsic measures

Evaluation is a crucial step in SSM, facilitating comparison between models and assessing suitability for application. In a clinical setting, where ground truth knowledge exists, this may be facilitated through extrinsic methods. Qualitative evaluation methods [16] include visualizing modes of variation to determine if they align with clinically relevant variations. Additionally, cluster analysis can be used to test the model's ability to detect known natural groups within the data. For quantitative evaluation, models can be used to infer patient-specific anatomical morphometrics automatically [7]. This is performed by manually defining landmarks and measurements on the model's mean shape and then using the model's correspondences to map these to individual patients. The model's accuracy can then be evaluated by comparing its predictions to ground truth data. Typically, Euclidean distances are used to compare landmark positions, while absolute differences are used for measurements.

## 5.2. Intrinsic measures

The choice of correspondence points is critical to a model's performance. In the absence of a ground truth, models can be evaluated intrinsically by their compactness, generalization and specificity; proposed by Davies [39], these metrics are determined by the location of correspondence points in a model and the modes of variation (PCs) derived from PCA (figure 3).

### 5.2.1. Compactness

A more compact model implies that the correspondence points used to construct it are superior, such that the model captures more variability in geometry using fewer PCs [30]. Mathematically, compactness is calculated by summing the variance of the first $M$ PCs in a PDM [39], as follows:

$$C(M) = \sum_{i=1}^{M} \lambda_i, \tag{5.1}$$

where $\lambda_i$ is the $i$th eigenvalue from the covariance matrix.

### 5.2.2. Generalization

Generalization is a measure of the model's ability to represent unseen geometries [30]. This is assessed using 'leave-one-out' cross-validation. A model is built using all but one geometry from a population. The model is then tested by measuring how well it can describe the excluded geometry. This process is repeated, excluding a different geometry in the population each turn, with approximation error averaged over the whole population. Mathematically, this is defined as [39]

$$G(M) = \frac{1}{n}\sum_{i=1}^{n} \epsilon_i^2(M), \tag{5.2}$$

where $n$ is the number of geometries, and $\epsilon_i^2(M)$ is the approximation error, based on the root mean squared Euclidean distance, using the first $M$ PCs in a PDM with excluded geometry.

### 5.2.3. Specificity

Specificity refers to the ability of a model to generate new, plausible geometries [30]. New geometries are calculated using the first $M$ eigenvectors in a PDM, assuming a multivariate normal distribution. Their Euclidean distance to the closest training sample is then calculated. Mathematically, this is defined as [39]

$$S(M) = \frac{1}{n}\sum_{i=1}^{n} |S_i - S_i'|^2, \tag{5.3}$$

where $M$ is the number of PCs in the PDM, $n$ is the number of randomly generated geometries, $S_i$ is a randomly generated geometry vector, and $S_i'$ is the geometry vector within the population with shortest Euclidean distance to $S_i$.

## 5.3. Pairwise versus groupwise approaches

In a comprehensive study, Goparaju *et al.* [7] compared the performance of ShapeWorks and SPHARM-PDM using shape models derived from 130 left atrial appendage (LAA) geometries. The study used a robust methodology, using a 70–30 split for training and testing, with two random iterations to ensure reliability. The results consistently favored ShapeWorks across multiple evaluation metrics. ShapeWorks demonstrated superior model compactness compared with SPHARM-PDM. In terms of generalization ability, ShapeWorks performed comparably to SPHARM-PDM in one split and outperformed it in the other. As the number of modes increased in one of the splits, ShapeWorks exhibited increasing specificity, surpassing SPHARM-PDM's performance. Perhaps most significantly, ShapeWorks successfully identified clinically relevant modes of variation in the data, specifically elongation of the appendage and ostia size. In contrast, SPHARM-PDM failed to accurately capture either the representative shape or the dominant modes of variation. Furthermore, ShapeWorks demonstrated the ability to detect natural clusters within the data, a crucial feature for understanding underlying patterns in anatomical structures. These findings underscore the importance of methodology in SSM and highlight the potential of groupwise correspondence approaches in capturing clinically relevant anatomical variations.

## 5.4. Task-level validation

When SSM-derived features are used for clinical association or prediction, validation should proceed at the task level with explicit statistical safeguards. While PCA itself does not require normality, distributional assumptions become relevant once probabilistic interpretations or parametric tests/regression are applied to PC scores [37]. Good practice is to examine the score distributions and consider transformations or robust estimators if non-Gaussian.

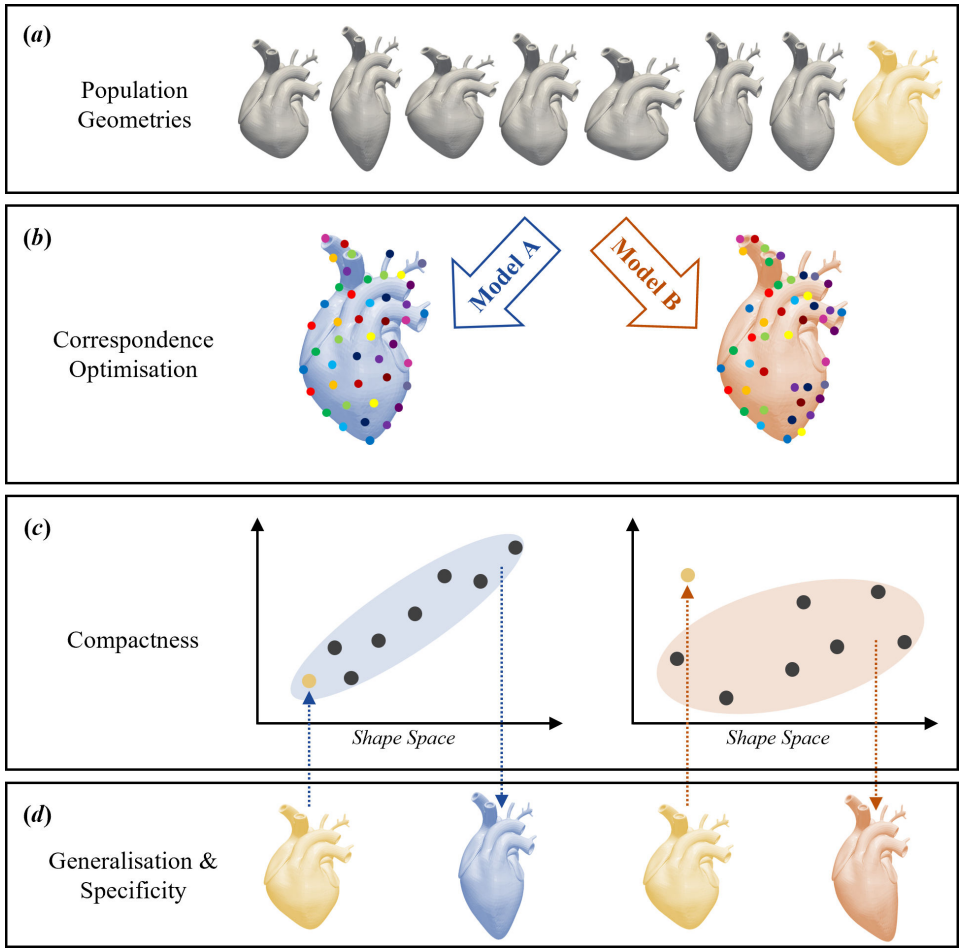


**Figure 3.** Intrinsic evaluation metrics. These metrics depend on correspondence point placement and PCA-derived modes of variation. (*a*) Population of geometries, with those in grey used to develop the models. (*b*) Correspondence optimization, with Model A achieving a more uniform distribution. (*c*) Shape space representation, where Model A is more compact, needing fewer PC modes to describe shape variability. (*d*) Model A is more generalisable, being able to represent the unseen geometry (illustrated in yellow), and more specific, generating plausible new geometries.

Evaluation should pre-specify endpoints and a clear analysis plan, use appropriate data splits (with temporal or geographical external test sets whenever feasible), and tune hyperparameters (including the number of retained modes) using nested cross-validation to reduce optimistic bias. To prevent data leakage, all steps that depend on the data distribution (segmentation refinements, alignment and correspondence optimization) should be performed within each training fold only, with test folds held out until final evaluation. Multiple testing should be addressed when interrogating many PC modes (e.g. false discovery rate control). While not an exhaustive list, considering such safeguards makes inferences from SSM-derived features statistically defensible and clinically applicable.

# 6. Clinical applications

## 6.1. Existing cardiac statistical shape models

SSM has emerged as a powerful tool in cardiovascular medicine, offering numerous applications across diagnosis, treatment and research (tables 1 and 2). The foundation to many of these applications is using SSM to define a normal range of anatomical variation, which requires a sufficiently large sample population [3].

In a bid to improve access to such sample data, the Cardiac Atlas Project (CAP) [73] exists as a large, sharable and web-accessible database of imaging examinations and associated clinical data. Multiple studies have used data from the CAP to understand geometric variability and produce openly accessible models. For example, Medrano-Gracia *et al.* [48] published a model of the left ventricle (LV) derived from 1991 healthy participants' magnetic resonance imaging (MRI), finding that the dominant modes of variability were size, sphericity at end-diastole, and concentricity at end-systole; modes of shape variability were able to distinguish differences due to clinical and demographic variables with greater statistical power than traditional mass and volume measurements. A similarly rich database is that of the UK Biobank, and this has led to the development of a biventricular shape model from 4329 MRI scans [74]. A biventricular model has also been published by Bai *et al.* [75], derived from 1093 MRI scans.

In regard to the other cardiac structures, multiple whole heart models have been published [76–79] alongside models of individual structures such as the atria or great vessels. These will be discussed in further detail in the subsequent sections.

**Table 1.** Summary of cardiovascular studies applying statistical shape modeling, organized by disease. AF, atrial fibrillation; CABG, coronary artery bypass graft; CAVC, complete atrioventricular canal; CFD, computational fluid dynamics; CoA, coarctation of the aorta; CRT, cardiac resynchronization therapy; HCM, hypertrophic cardiomyopathy; LA, left atrium; LAA, left atrial appendage; LV, left ventricle; LVSD, left ventricular systolic dysfunction; MI, myocardial infarction; PH, pulmonary hypertension; RV, right ventricle; RVOT, right ventricular outflow tract; TAVI, transcatheter aortic valve implantation; TOF, tetralogy of Fallot; VSD, ventricular septal defect.

| disease category | specific condition | study | key findings | clinical implications |
|---|---|---|---|---|
| arrhythmia | AF | Bieging *et al.* [40] | LAA shape features associated with stroke | improved risk stratification |
| | | Nagel *et al.* [41] | virtual population of bi-atrial anatomies | *in silico* trials |
| | | Jia *et al.* [42] | LA shape features associated with catheter ablation outcomes | improved patient selection |
| | | Bhalodia *et al.* [43] | LA and LAA shape features associated with stroke | improved risk stratification |
| | | Bieging *et al.* [44] | LA shape features associated with catheter ablation outcomes | improved patient selection |
| | | Goparaju *et al.* [16] | LAA shape variability | improved closure device design |
| | | Higuchi *et al.* [45] | spatial distribution of LA fibrosis | improved understanding of pathophysiology |
| | | Varela *et al.* [46] | LA shape features associated with catheter ablation outcomes | improved patient selection |
| | | Cates *et al.* [13] | LA shape features associated with AF type | improved understanding of pathophysiology |
| coronary artery disease | CABG | Bademci *et al.* [47] | proximity of main pulmonary artery to the sternum in patients with previous CABG | improved surgical approaches during re-sternotomy procedures |
| | coronary anatomy | Medrano-Gracia *et al.* [48] | coronary shape variability | improved coronary stent design |
| | post-MI LV aneurysm | Goubergrits *et al.* [49] | hemodynamics in template aneurysmal and non-aneurysmal LV geometries | improved translation of CFD modeling to clinical application |
| | post-MI LVSD | Zhang *et al.* [50] | LV shape features associated with negative remodeling following MI | improved risk stratification |
| | post-MI VSD | Asif *et al.* [51] | VSD shape variability | improved closure device design |
| cardiomyopathy | HCM | Hermida *et al.* [52] | LV shape features associated with HCM | improved diagnosis and risk stratification |
| | | Bernardino *et al.* [53] | biventricular shape features associated with physiological cardiac remodeling | improved diagnosis (distinguishing from athlete's heart) |
| | Takotsubo cardiomyopathy | Pontecorboli *et al.* [54] | LV shape features associated with early remodeling in Takotsubo | improved understanding of pathophysiology |
| congenital heart disease | CAVC defects | Nam *et al.* [55] | shape features of CAVC annulus vs. normal MV annulus | improved surgical approaches during valve repair |
| | CoA | Minderhoud *et al.* [26] | aortic shape features associated with cardiovascular events | improved risk stratification |
| | | Hermida *et al.* [56] | virtual population of fetal CoA anatomies | *in silico* trials |
| | | Ardakani *et al.* [57] | hemodynamics in template CoA geometries | improved translation of CFD modeling to clinical application |

(*Continued.*)

**Table 1.** (*Continued.*)

| disease category | specific condition | study | key findings | clinical implications |
|---|---|---|---|---|
| | | Sophocleous *et al.* [58] | LV shape features associated with LV strain | improved understanding of pathophysiology |
| | | Sophocleous *et al.* [27] | aortic shape features associated with clinical measures | improved risk stratification |
| | | Bruse *et al.* [24] | aortic shape features associated with clinical measures | improved risk stratification |
| | | Bruse *et al.* [25] | aortic shape features associated with clinical measures | improved risk stratification |
| | hypoplastic left heart syndrome | Wong *et al.* [59] | ventricular shape features associated with clinical measures | improved risk stratification |
| | | Bruse *et al.* [60] | aortic shape features associated with clinical measures | improved risk stratification |
| | TOF | Kollar *et al.* [61] | RV shape features associated with hemodynamics | improved understanding of pathophysiology |
| | | Louvelle *et al.* [62] | RVOT and pulmonary artery shape features associated with hemodynamics | improved understanding of pathophysiology |
| | | Leonardi *et al.* [63] | RV shape features associated with clinical measures | improved risk stratification |
| heart failure | Anthracycline- related LVSD | Narayan *et al.* [64] | LV shape features associated with clinical history | improved diagnosis and risk stratification |
| | CRT | Warriner *et al.* [65] | pre-CRT LV shape features associated with clinical outcomes | improved patient selection |
| valvular heart disease | aortic valve | Asheghan *et al.* [66] | LV shape features associated with TAVI outcomes | improved patient selection |
| | | Verstraeten *et al.* [67] | virtual population of aortic valve stenosis anatomies | *in silico* trials |
| | | Cutugno *et al.* [68] | LV shape features associated with clinical outcomes | improved patient selection |
| | | Bosmans *et al.* [69] | aortic root shape features and TAVI device selection associated with outcomes | improved device selection |
| | mitral valve | Lopes *et al.* [70] | accurate, automated measurement for transcatheter mitral valve replacements | improved procedural planning |
| | tricuspid valve | Orkild *et al.* [71] | RV shape features associated with tricuspid regurgitation | improved diagnosis and risk stratification |
| vascular disease | PH | Orkild *et al.* [71] | RV shape features associated with PH | improved diagnosis and risk stratification |
| | | Xu *et al.* [72] | RV shape features associated with PH | improved diagnosis and risk stratification |

## 6.2. Diagnosis and risk stratification

SSM has demonstrated significant potential in enhancing the diagnosis of CVDs and stratifying patient risk, being successfully applied to identify shape features associated with various cardiac conditions. By quantifying subtle shape variations that may not be apparent through traditional clinical measures, models can identify pathological patterns and predict disease progression.

### 6.2.1. Biventricular models

Bernardino *et al.* [53] sought to assess biventricular changes in athletes compared with non-athletes, the need to differentiate between pathological and physiological cardiac remodeling being crucial in clinical practice. Their analysis of MRI data from 89 triathlon athletes and 77 healthy controls revealed that remodeling in athletes was characterized by a shift in right ventricular

**Table 2.** Statistical shape-modeling methodology and software used for studies listed in table 1. SSM: statistical shape modeling.

| SSM approach | details / software | study | N | compactness (modes, variance) |
|---|---|---|---|---|
| point distribution model | groupwise, ShapeWorks | Bhalodia *et al.* [43] | 243 | 13, 95% |
| | | Bieging *et al.* [44] | 254 | 19, 90% |
| | | Bieging *et al.* [40] | 244 | 10, 91.7% |
| | | Cates *et al.* [13] | 137 | 8, 95% |
| | | Goparaju *et al.* [16] | 130 | 11, 95% |
| | | Higuchi *et al.* [45] | 160 | not reported |
| | | Orkild *et al.* [71] | 78 | 31, 99% |
| | groupwise, other | Bademci *et al.* [47] | 40 | not reported |
| | | Cutugno *et al.* [68] | 86 | 8, 90% |
| | | Hermida *et al.* [52] | 2398 | 25, 91% |
| | | Hermida *et al.* [56] | 112 | 10, 86% |
| | | Nam *et al.* [55] | 100 | not reported |
| | | Xu *et al.* [72] | 50 | 15, 98% |
| | pairwise, SPHARM-PDM | Goparaju *et al.* [16] | 130 | 18, 95% |
| | pairwise, ScalismoLab | Nagel *et al.* [41] | 47 | 24, 95% |
| | pairwise, other | Asheghan *et al.* [66] | 66 | 5, 95% |
| | | Bernardino *et al.* [53] | 166 | not reported |
| | | Bosmans *et al.* [69] | 35 | not reported |
| | | Goubergrits *et al.* [49] | 125 | 30, 90% |
| | | Lopes *et al.* [70] | 50 | not reported |
| | | Medrano-Gracia *et al.* [48] | 211 | 3, 71% |
| | | Narayan *et al.* [64] | 20 | 5, 76% |
| | | Varela *et al.* [46] | 144 | 8, 84.6% |
| | | Warriner *et al.* [65] | 50 | not reported |
| | | Wong *et al.* [59] | 93 | 10, 79% |
| | | Zhang *et al.* [50] | 2291 | 20, 90% |
| deformation field | Deformetrica | Asif *et al.* [51] | 15 | not reported |
| | | Goparaju *et al.* [16] | 130 | 13, 95% |
| | | Jia *et al.* [42] | 141 | not reported |
| | | Kollar *et al.* [61] | 36 | 10, 80% |
| | | Minderhoud *et al.* [26] | 65 | not reported |
| | | Sophocleous *et al.* [27] | 108 | 9, 72% |
| | | Sophocleous *et al.* [58] | 110 | 5, 54% |
| | | Verstraeten *et al.* [67] | 97 | 32, 91% |
| | other | Bruse *et al.* [24] | 20 | 2, 43% |
| | | Bruse *et al.* [25] | 53 | not reported |
| | | Bruse *et al.* [60] | 37 | not reported |
| | | Ardakani *et al.* [57] | 108 | not reported |
| | | Leonardi *et al.* [63] | 38 | 20, 95% |
| | | Louvelle *et al.* [62] | 16 | 6, 80% |
| | | Pontecorboli *et al.* [54] | 28 | not reported |

(RV) volume distribution towards the infundibulum, increased overall RV volume and increased LV mass. This application of SSM holds particular value in distinguishing between athlete's heart and pathological conditions like hypertrophic cardiomyopathy (HCM) or arrhythmogenic cardiomyopathy, where current clinical measurements may not be sufficiently discriminating.

### 6.2.2. Left ventricular models

Multiple studies have focused on LV remodeling in specific diseases. Zhang *et al.* [50] demonstrated the utility of SSM in quantifying LV remodeling after myocardial infarction (MI). Their study, which included 300 patients with MI and 1991 healthy controls from the CAP, showed that SSM-based shape parameter analysis could characterize remodeling features associated with MI more effectively than existing measures of end-diastolic and end-systolic volume, and LV mass. Using these shape parameters may identify patients with more adverse remodeling, requiring more aggressive treatment. Narayan *et al.* [64] explored anthracycline-related LV dysfunction. By comparing MRI data from 20 patients previously treated with high- or low-dose anthracyclines and the healthy LV model of Medrano-Gracia [48], they identified shape modes corresponding to lower overall size and sphericity in treated patients. Furthermore, the study demonstrated that the addition of shape-based measures significantly improved the ability of conventional measures to discriminate between individuals who received low or high dose anthracycline. As such, shape-based LV measures may be able to improve the detection of anthracycline cardiac toxicity. Hermida *et al.* [52] investigated obstruction in HCM, using 2298 patients' MRI data. They found HCM to be associated not only with the previously established measure of basal septal hypertrophy, but additionally with LV lengthening, apical dilatation, and narrowing of the LV outflow tract. Cutugno *et al.* [68] studied the association of LV shape with aortic stenosis. Comparing CT data from 30 control and 65 aortic stenosis patients, they were able to develop a shape-based predictive classification tool of the need for valvular intervention, which outperformed one based on clinical and demographic indicators. Pontecorboli *et al.* [54] investigated Takotsubo cardiomyopathy, their MRI-based analysis of 28 patients demonstrating that early LV remodeling in Takotsubo is mainly related to changes in size rather than sphericity, providing insights into its pathophysiology.

### 6.2.3. Right ventricular models

In a study on RV remodeling, Orkild *et al.* [71] compared 41 patients with tricuspid regurgitation due to pulmonary hypertension (PH) or congestive heart failure, 31 comorbidity-matched controls without tricuspid regurgitation and six healthy controls. They observed that tricuspid regurgitation, regardless of aetiology, led to similar RV shape changes and that these could be used to reliably identify patients with regurgitation. Moreover, they found that the RV in patients with PH without tricuspid regurgitation had distinct shape features; as such, RV shape may be particularly valuable in defining the severity of PH. In a further study on PH, Xu *et al.* [72] compared 33 patients with PH and 17 non-PH control patients, analysing both MRI-based shape data and hemodynamic data from right heart catheter studies. They identified two shape modes related to PH state: RV free wall expansion and septal flattening. Notably, the latter was significantly correlated with clinical outcomes, outperforming hemodynamic variables in predicting prognosis. Their identified shape descriptors may provide the basis for future, non-invasive strategies for identifying patients with PH and decompensating RVs.

### 6.2.4. Atrial models

Cates *et al.* [13] investigated left atrial (LA) shape in atrial fibrillation (AF). Through comparison of MRI scans from 37 control subjects, 50 patients with paroxysmal AF and 50 patients with persistent AF, they were able to identify anteroposterior dilation as the most significant shape change between groups. This supported previous evidence of LA remodeling that identified asymmetry index and LA sphericity as markers of disease [34,80]. Regarding stroke risk in AF, both Bhalodia *et al.* [43] and Bieging *et al.* [40] investigated the impact of LA and LAA shape. The former identified the importance of the relative alignment between the LA and LAA, the latter that a broader, shorter and less angulated LAA increased risk of stroke; combining shape parameters with $CHA_2DS_2$-VASc score significantly improved risk prediction compared with $CHA_2DS_2$-VASc score alone.

## 6.3. Treatment

SSM has found valuable applications in the treatment of CVDs, notably in the context of device-based therapy and surgical procedures. Here, shape can inform treatment planning, optimize its delivery and guide follow-up.

### 6.3.1. Predicting treatment response

SSM has shown promise in predicting treatment response across various cardiovascular interventions. Asheghan *et al.* [66] combined machine learning (ML) and SSM to predict LV mass index regression following transcatheter aortic valve implantation (TAVI) based on pre-treatment imaging of the LV in patients with severe aortic stenosis. Their model, based on CT images from 66 patients, demonstrated the potential of shape modeling as a tool for predicting post-intervention outcomes. Warriner *et al.* [65] used SSM to predict response to cardiac resynchronization therapy (CRT). Their analysis of 50 patients' MRI data revealed that specific pre-CRT LV shape features, such as asymmetric wall thickness, were independent predictors of favorable remodeling response to CRT. Multiple studies have investigated LA shape as a predictor of recurrence following catheter ablation treatment of AF, generally finding recurrent atria to be more spherical in shape [42,44,46]. Furthermore, Bieging *et al.* [44] were able to demonstrate the additional value of shape information in combination with fibrosis quantification for predicting recurrence.

### 6.3.2. Treatment optimization

SSM has been applied to optimize the sizing and selection of transcatheter valves. Bosmans *et al.* [69] used SSM to analyze the aortic root on pre-procedural CT scans of 35 patients with TAVI. They found correlations between specific shape components and implant size, as well as associations between certain shape features and post-procedure paravalvular regurgitation. Lopes *et al.* [70] demonstrated the feasibility of using SSM to automate measurements for transcatheter mitral valve replacements. Their study, based on CT scans of 50 patients, showed that SSM-derived measurements were in close agreement with expert manual analysis, offering potential benefits in terms of consistency and time efficiency in procedure planning.

SSM has potential applications in optimizing LAA closure device selection. While current patient selection criteria for LAA exclusion are mainly based on clinical information, Shin and Park [81] suggested that SSM could help characterize individual patients' thrombotic risk based on LAA anatomical characteristics and surrounding hemodynamics, potentially informing more personalized decision-making regarding this treatment.

SSM has been used in planning for various cardiac surgical procedures. Nam *et al.* [55] analyzed the structure of the atrioventricular canal annulus in patients with complete atrioventricular canal (CAVC) defects. Their findings on the planarity of the left side of the native CAVC annulus compared with the normal mitral annulus may have implications for optimizing surgical repair techniques. Bademci *et al.* [47] applied SSM to study the retrosternal area in patients with previous coronary artery bypass grafting (CABG). Their findings on the proximity of the main pulmonary artery to the sternum post-CABG could inform surgical approaches during re-sternotomy procedures.

### 6.3.3. Treatment follow-up

SSM offers a valuable tool for monitoring disease progression and assessing treatment response. Wong *et al.* [59] compared the effects of two different Norwood procedure techniques on ventricular shape and function in hypoplastic left heart syndrome patients. Their study analyzed 93 MRI scans, with 59 patients having a modified Blalock–Taussig (MBT) shunt and 34 having a right ventricle-to-pulmonary artery (RVPA) conduit. They observed that patients who had undergone RVPA conduit insertion had focal scarring and volume loading, suggesting the need for continued surveillance post-procedure. Leonardi *et al.* [63] used SSM to correlate three-dimensional RV shape with clinical metrics in repaired tetralogy of Fallot (TOF) patients. Their analysis provided new insights into RV adaptation to chronic pulmonary insufficiency and suggested that RV shape biomarkers could guide personalized follow-up of these patients.

Multiple studies have focused on patients with previous coarctation of the aorta (CoA) repair. Distinct shape features have been identified that relate to clinically significant markers such as ejection fraction and LV mass [24,25,27]. Additionally, these patients have been demonstrated to have more tortuous aortic arches compared with controls, and this has been associated with cardiovascular events [26]. The aortic arch has also been studied in the context of hypoplastic left heart syndrome palliation with total cavopulmonary connection [58]. Findings suggested that altered aortic morphology in these patients has important associations with higher superior cavopulmonary pressure and short-term outcomes after the procedure.

## 6.4. Research

By relating shape to function and identifying shape features associated with specific pathologies, SSM contributes to our understanding of mechanisms in CVD. Furthermore, integration of mathematical and statistical models of morphology and physiology has been pivotal in understanding both the normal and pathological function of the heart [73].

### 6.4.1. Understanding disease mechanisms

Studies have used SSM to correlate shape features with functional parameters. Sophocleous *et al.* [58] studied LV shape in patients with CoA, their analysis of MRI revealed an association between increasing LV sphericity and reduced LV strain indices, suggesting that variation in shape has functional implications. Farrar *et al.* [82] studied eight patients with a previous Fontan procedure, demonstrating significant relationships between ventricular shape and wall motion abnormalities. Kollar *et al.* [61] used MRI-based four-dimensional flow imaging to demonstrate the relationship between RV shape and hemodynamic forces in patients with repaired TOF. A study by Cates *et al.* [13] used a combination of MRI and transthoracic echocardiogram data to compare LAA morphology in patients with and without spontaneous echo contrast (SEC) within the LAA; they observed SEC to be more prevalent in longer and thinner LAAs that curved anteriorly away from the LA body.

Expanding on analyzes of shape and hemodynamics, several studies have combined SSM with computational fluid dynamics (CFD). Louvelle *et al.* [62] investigated repaired TOF patients, linking SSM-derived shape parameters to energy efficiency metrics derived from CFD simulations in 16 paediatric patients. Rather than using personalized CFD modeling, Khalafvand *et al.* [83] used SSM to derive five characteristic LV shapes from 150 patients. CFD on these was used to gain insight into the interplay of LV shape and blood flow dynamics. Similarly, in the study of LV aneurysms, Goubergrits *et al.* [49] used CFD to simulate intracardiac flow in seven template geometries derived from the CT data of 125 patients post-MI. Ardakani *et al.* [57] investigated CoA, deriving template geometries for repaired CoA, unrepaired CoA, and no CoA. CFD in each template revealed that small alterations in aortic morphology can have significant impacts on important hemodynamic metrics. Given the computational cost of CFD, approaches using template geometries may aid in clinical translation, as patients may be classified to one of these templates rather than requiring patient-specific simulations.

Template geometries can also aid in the visualization of research measures, producing spatial histograms. For example, Higuchi *et al.* [45] used a template LA geometry to explore the spatial distribution of fibrosis in 160 patients with AF. Complementary approaches were used by Sharp *et al.* [84], Nairn *et al.* [85], and Azzolin *et al.* [86], who derived template LA geometries to facilitate the comparison of measurements made using different modalities, without variations due to spatial displacement. Furthermore, in the field of electrophysiology, SSM has been combined with electrophysiological simulations to explore the impact of segmentation variability on electrocardiographic imaging (ECGI) mapping [87,88].

### 6.4.2. Device design

SSM has contributed significantly to the field of cardiac device design and development. Medrano-Gracia *et al.* [89] used SSM-based analysis of CT data from 211 patients with no history of coronary artery disease to better understand shape variability at coronary artery bifurcations. Their findings on vessel size, bifurcation angles and inlet curvature angles could inform more anatomically optimized stent designs. Bruse *et al.* [90] studied the geometry of extra-cardiac conduit vascular grafts in patients with Fontan circulation, providing insights that could inform the design and placement of cavopulmonary assist devices. Asif *et al.* [51] analyzed the morphology of post-infarction ventricular septal defects, suggesting that knowledge of morphological variability could inform both device sizing and design for these challenging cases. Goparaju *et al.* [16] investigated LAA morphology in 130 patients with AF, demonstrating the potential of SSM in informing the design of closure devices through population-level statistics, categorizing LAA morphologies without the subjective error encountered when performing this manually.

### 6.4.3. Virtual populations

Through randomly selecting weights for each shape mode from a normal distribution, statistical shape models have the ability to generate plausible variations of cardiac anatomy, making them valuable tools for creating virtual patient populations [3]. Such cohorts can be used for *in silico* trials; for example, Verstraeten *et al.* [67] generated synthetic aortic valve stenosis geometries for *in silico* TAVI trials, showcasing their potential in device testing and optimization.

This is particularly valuable in the case of rare anatomical variants; for example, Hermida *et al.* [56] used a model derived from MRI data of 112 fetuses with suspected CoA to generate a virtual cohort of 1000 openly available synthetic cases. A further advantage has been highlighted by Nagel *et al.* [6], who developed and used a bi-atrial SSM to generate 100 virtual bi-atrial anatomies. Rule-based augmentation was used to add wall thickness, inter-atrial bridges, and fibre orientation, with subsequent ECG simulations consistent with observational data from large cohort studies. Such an automated approach negates the need for time-consuming and labour-intensive segmentation and model generation from individual patients' imaging data.

A powerful use case of such virtual populations is in the training of ML models, where they may overcome limitations of real-world data availability, particularly when combined with other forms of computational modeling. Thamsen *et al.* [91] generated a virtual population of 2652 CoA cases with both morphological data and hemodynamic data using CFD. The model of Rodero *et al.* [78] has been used by Kim *et al.* [92] to train a ML model to detect apical foreshortening on two-dimensional echocardiogram images, and by Zolotarev *et al.* [93] to train a ML model to predict the impact of different AF ablation strategies. In the context of AF, Nagel *et al.* [41] also used a virtual population derived from their group's model [6] to train a ML model to predict the amount of atrial fibrosis from the P wave of a 12-lead ECG.

An important caveat is that synthetic cases sampled from a single statistical shape model are draws from the same generative fit and therefore are not independent observations in the epidemiological sense. The information content of any synthetic cohort is bounded by the size, diversity and measurement quality of the real cohort used for SSM; increasing the virtual cohort size can drive classical $p$-values arbitrarily low without adding new biological evidence. Accordingly, when used for hypothesis testing, emphasis should be placed on effect sizes, the virtual sample size should be reported alongside the size of the underlying real cohort, and the virtual sample size limited to that needed for numerical stability rather than inference. Finally, results obtained with synthetic populations, whether for *in silico* trials or ML training, should be validated on held-out real patients.

## 7. Challenges and future directions

### 7.1. Clinical uptake

SSMs are often presented through a mean shape and PC modes of variation. If analyzes stop at comparing mean shapes, granularity is lost and any inferences are necessarily group level. Uptake of SSM into routine clinical care requires more concrete benefit. In part, this can be provided through improved mechanistic insight into why a particular morphology relates to physiology or risk. Coupling SSMs with additional tools to provide mechanistic explanations (§6.4.1) is one approach that can move SSM findings from descriptive to ultimately actionable.

It is also important to recognize that SSM can support patient-specific use, since each individual is represented by a subject-specific coefficient vector in the learnt shape space that quantifies deviation from the mean across modes. These embeddings can drive subject-level inference, prediction and decision support when linked to clinical labels or physiological surrogates with appropriate supervised models. The practical limitation is not that SSMs are inherently non-individualized, but that low-dimensional truncation or coarse correspondences may discard clinically relevant nuance, and that group associations

can be mistakenly extrapolated to individuals, the ecological fallacy, without proper validation. Prospective evidence that an approach changes decisions or improves outcomes is therefore critical to gain the trust of clinicians [94].

Despite these challenges, there are already clinical products deploying SSM-based approaches. Examples include Philips HeartModel AI, which uses 'anatomical intelligence' to automate LV and LA quantification from three-dimensional echocardiography [95], and Corify's DYNAMO framework, which employs a bi-atrial SSM for ECGI [96]. These examples highlight a practical route that emphasizes tightly scoped, well-validated, model-based tools embedded within clinical platforms, accompanied by transparent performance reporting and ongoing post-deployment monitoring.

### 7.2. Multi-label and multi-organ models

Most models discussed thus far focus on a single anatomical component of the heart. Yet, the structures that constitute cardiac anatomy are spatially, functionally and physiologically interconnected, so change in one part can influence the system as a whole. Multi-label models capture combinations of structures such as the left and right ventricles [53,74,75] or the whole heart [76–79], and such joint analyzes can reveal clinically relevant remodeling patterns.

A central challenge for these approaches is the treatment of boundaries between structures, that is, the shared surfaces. In practice, models either treat each component separately and then apply a global alignment to enforce continuity at the boundaries, or they optimize correspondences jointly across all structures with constraints imposed on the surfaces that two structures have in common. Iyer *et al.* [97] introduced an explicit, consistently parametrized shared boundary surface within PDMs that adjusts the particle-based optimization, so particles interact with the interface without penetrating or separating from it. This yields anatomically consistent modes with no gaps, overlaps, or misalignment noise and is especially valuable when estimating biomarkers that are centred on the shared boundary. Applied to a biventricular dataset, the authors demonstrate septal-specific variation in conditions that raise RV pressure.

Further extending the multi-label concept, multi-organ models extend beyond the heart to consider the joint impact of CVD on related structures, for example, the great vessels. Progress in this direction reflects the field's broader ambition to represent interacting organs within a single statistical framework. For techniques and applications spanning multiple organs, the reader is directed to Cerrolaza *et al.* [98].

### 7.3. Deep-learning-based statistical shape modeling

A particular challenge in producing such multi-organ models is the existence of nonlinear variability in geometry within a population [98]. Consequently, deviation from the underlying assumption of Gaussian statistics limits the power of PCA to capture this variability [99].

In response to this challenge, deep-learning-based SSM approaches have emerged, such as DeepSSM, VIB-DeepSSM [100] and Mesh2SSM [4]. Deep learning methods create a condensed representation of complex input data in a lower-dimensional space, known as the latent space. This space aims to capture the essential features of the data efficiently, with each dimension in the latent space ideally representing a distinct aspect of how the data varies between subjects. The nonlinear nature of deep learning models offers a key benefit, allowing them to capture more sophisticated and compact relationships between the original high-dimensional data and its representation in the lower-dimensional latent space [101].

### 7.4. Spatio-temporal statistical shape modeling

Cardiac geometry is not static but undergoes dynamic changes through the cardiac cycle and over the course of disease progression; traditional SSM is limited in its ability to capture this variability. Spatio-temporal SSM integrates longitudinal shape measurement, allowing for the quantification and evaluation of temporal evolution in anatomical structures [5].

In the realm of dynamic motion analysis, Adams *et al.* [102] used a PSM-based optimization process on four-dimensional LA data of patients with AF. Although establishing both inter-subject and intra-subject correspondences, they were able to differentiate between cohort and temporal effects, respectively, and represent dynamic LA geometric changes. Similarly, a model by Beetz *et al.* [103] was developed to capture the mechanical deformation of complete three-dimensional ventricular geometry throughout the cardiac cycle. By analysing subject-specific motion patterns separately from morphology, these models can help identify abnormalities related to both dynamics and shape, providing invaluable insights into the impact of disease on mechanical function [104].

In tracking disease progression, spatio-temporal SSM allows for computation of shape trajectories representing average disease progression in a cohort; for example, Sophocleous et al. [105] studied the progression of aortic morphology in bicuspid aortic valve patients through serial MRI. Such an approach enables personalized treatment strategies that can adapt to a patient's evolving condition, identifying early signs of disease and monitoring the efficacy of interventions.

## 8. Conclusion

By providing quantitative insights into cardiac shape and its relationship to function and pathology, SSM stands as a powerful tool in the ongoing effort to improve cardiovascular care. As SSM techniques continue to evolve and integrate with other advanced computational methods, their role in cardiovascular medicine is likely to grow. Future developments will lead to

more comprehensive, accurate and clinically relevant models, further enhancing our understanding of cardiac anatomy and function in both health and disease. Thus, SSM is poised to play an increasingly important role in advancing personalized medicine, optimizing treatment strategies and ultimately improving patient outcomes in CVD.

Ethics. This work did not require ethical approval from a human subject or animal welfare committee.

Data accessibility. This article has no additional data.

Declaration of AI use. We have not used AI-assisted technologies in creating this article.

Authors' contributions. A.J.S.: conceptualization, data curation, formal analysis, funding acquisition, investigation, methodology, validation, visualization, writing—original draft, writing—review and editing; T.R.B.: funding acquisition, investigation, project administration, resources, supervision, writing—review and editing; A.B.: conceptualization, funding acquisition, investigation, methodology, project administration, resources, supervision, writing—review and editing.

All authors gave final approval for publication and agreed to be held accountable for the work performed therein.

Conflict of interest declaration. We declare we have no competing interests.

Funding. This work was supported by the Royal Society (URF\R1\221314) and Heart Research UK (NET25-100009).

# References


1. World Health Organization. Cardiovascular diseases (CVDs) – key facts. See https://www.who.int/news-room/fact-sheets/detail/cardiovascular-diseases-(cvds.
2. Luengo-Fernandez R *et al*. 2023 Economic burden of cardiovascular diseases in the European Union: a population-based cost study. *Eur. Heart J*. **44**, 4752–4767. (doi:10.1093/eurheartj/ehad583)
3. Ambellan F, Lamecker H, von Tycowicz C, Zachow S. 2019 Statistical shape models: understanding and mastering variation in anatomy. In *Biomedical visualisation* (ed. PM Rea), pp. 67–84. Cham, Switzerland: Springer International Publishing. (doi:10.1007/978-3-030-19385-0_5)
4. Iyer K, Elhabian S. 2023 Mesh2SSM: from surface meshes to statistical shape models of anatomy. *Med. Image Comput. Comput. Assist. Interv.* **14220**, 615–625. (doi:10.1007/978-3-031-43907-0_59)
5. Adams J, Khan N, Morris A, Elhabian S. 2022 Spatiotemporal cardiac statistical shape modeling: a data-driven approach. *Stat. Atlases Comput. Model. Heart STACOM* **13593**, 143–156. (doi:10.1007/978-3-031-23443-9_14)
6. Nagel C, Schuler S, Dössel O, Loewe A. 2021 A bi-atrial statistical shape model for large-scale in silico studies of human atria: model development and application to ECG simulations. *Med. Image Anal.* **74**, 102210. (doi:10.1016/j.media.2021.102210)
7. Goparaju A *et al*. 2022 Benchmarking off-the-shelf statistical shape modeling tools in clinical applications. *Med. Image Anal*. **76**, 102271. (doi:10.1016/j.media.2021.102271)
8. Adams DC, Rohlf FJ, Slice DE. 2004 Geometric morphometrics: ten years of progress following the 'revolution.' *Ital. J. Zool*. **71**, 5–16. (doi:10.1080/11250000409356545)
9. Piazzese C, Carminati MC, Pepi M, Caiani EG. 2017 Statistical shape models of the heart: applications to cardiac imaging. In *Statistical shape and deformation analysis* (eds G Zheng, S Li, G Székely), pp. 445–480. Cambridge, MA: Academic Press. (doi:10.1016/B978-0-12-810493-4.00019-5)
10. Cootes TF, Taylor CJ, Cooper DH, Graham J. 1995 Active shape models—their training and application. *Comput. Vis. Image Underst.* **61**, 38–59. (doi:10.1006/cviu.1995.1004)
11. Stegmann MB, Gomez DD. 2002 *A brief introduction to statistical shape analysis*. Lyngby, Denmark: Informatics and Mathematical Modelling, Technical University of Denmark, DTU. See https://www2.imm.dtu.dk/pubdb/edoc/imm403.pdf.
12. Davies RH, Twining CJ, Cootes TF, Waterton JC, Taylor CJ. 2002 A minimum description length approach to statistical shape modeling. *IEEE Trans. Med. Imaging* **21**, 525–537. (doi:10.1109/TMI.2002.1009388)
13. Cates J, Bieging E, Morris A, Gardner G, Akoum N, Kholmovski E, Marrouche N, McGann C, MacLeod RS. 2014 Computational shape models characterize shape change of the left atrium in atrial fibrillation. *Clin. Med. Insights Cardiol.* **8**, 99–109. (doi:10.4137/CMC.S15710)
14. Heitz G, Rohlfing T, Maurer Jr. CR. 2005 Statistical shape model generation using nonrigid deformation of a template mesh. In *Proc. SPIE 5747, Medical Imaging*, San Diego, CA, p. 1411. (doi:10.1117/12.594802)
15. Cates J, Fletcher PT, Styner M, Shenton M, Whitaker R. 2007 Shape modeling and analysis with entropy-based particle systems. *Inf. Process. Med. Imaging* **20**, 333–345. (doi:10.1007/978-3-540-73273-0_28)
16. Goparaju A, Csecs I, Morris A, Kholmovski E, Marrouche N, Whitaker R, Elhabian S. 2018 On the evaluation and validation of off-the-shelf statistical shape modeling tools: a clinical application. In *Lecture notes in computer science shape in medical imaging* (eds M Reuter, C Wachinger, H Lombaert, B Paniagua, M Lüthi, B Egger), pp. 14–27. Cham, Switzerland: Springer International Publishing. (doi:10.1007/978-3-030-04747-4_2)
17. Oguz I, Cates J, Datar M, Paniagua B, Fletcher T, Vachet C, Styner M, Whitaker R. 2016 Entropy-based particle correspondence for shape populations. *Int. J. Comput. Assist. Radiol. Surg*. **11**, 1221–1232. (doi:10.1007/s11548-015-1319-6)
18. Paulsen R, Larsen R, Nielsen C, Laugesen S, Ersbøll B. 2002 Building and testing a statistical shape model of the human ear canal. In *Medical image computing and computer-assisted intervention — MICCAI 2002* (eds T Dohi, R Kikinis), vol. **2489**. Berlin, Germany: Springer.(Lecture Notes in Computer Science). (doi:10.1007/3-540-45787-9_47)
19. Styner M, Oguz I, Xu S, Brechbuehler C, Pantazis D, Levitt JJ, Shenton ME, Gerig G. 2006 Framework for the statistical shape analysis of brain structures using SPHARM-PDM. *Insight J*. (doi:10.54294/owxzil)
20. Cates J, Elhabian S, Whitaker R. 2017 ShapeWorks: particle-based shape correspondence and visualization software. In *Statistical shape and deformation analysis* (eds G Zheng, S Li, G Székely), pp. 257–298. Cambridge, MA: Academic Press. (doi:10.1016/B978-0-12-810493-4.00012-2)
21. Adams J, Elhabian S. 2022 From images to probabilistic anatomical shapes: a deep variational bottleneck approach. *Med. Image Comput. Comput. Assist. Interv.* **13432**, 474–484. (doi:10.1007/978-3-031-16434-7_46)
22. Avants BB, Tustison NJ, Song G, Cook PA, Klein A, Gee JC. 2011 A reproducible evaluation of ANTs similarity metric performance in brain image registration. *NeuroImage* **54**, 2033–2044. (doi:10.1016/j.neuroimage.2010.09.025)
23. Durrleman S, Prastawa M, Charon N, Korenberg JR, Joshi S, Gerig G, Trouvé A. 2014 Morphometry of anatomical shape complexes with dense deformations and sparse parameters. *NeuroImage* **101**, 35–49. (doi:10.1016/j.neuroimage.2014.06.043)
24. Bruse JL *et al*. 2016 A statistical shape modelling framework to extract 3D shape biomarkers from medical imaging data: assessing arch morphology of repaired coarctation of the aorta. *BMC Med. Imaging* **16**, 40. (doi:10.1186/s12880-016-0142-z)

25. Bruse JL *et al*. 2017 How successful is successful? Aortic arch shape after successful aortic coarctation repair correlates with left ventricular function. *J. Thorac. Cardiovasc. Surg.* **153**, 418–427. (doi:10.1016/j.jtcvs.2016.09.018)
26. Minderhoud SCS *et al*. 2024 Aortic geometry and long-term outcome in patients with a repaired coarctation. *Open Heart* **11**, e002642. (doi:10.1136/openhrt-2024-002642)
27. Sophocleous F *et al*. 2019 Aortic morphological variability in patients with bicuspid aortic valve and aortic coarctation. *Eur. J. Cardio Thorac. Surg*. **55**, 704–713. (doi:10.1093/ejcts/ezy339)
28. Dryden IL, Mardia KV. 2016 *Statistical shape analysis, with applications in R*, 2nd edn. Chichester, UK: John Wiley & Sons. (doi:10.1002/9781119072492)
29. Kendall DG, Barden D, Carne T, Le H. 2009 *Shape and shape theory*. Chichester, UK: John Wiley & Sons.
30. Munsell BC, Dalal P, Wang S. 2008 Evaluating shape correspondence for statistical shape analysis: a benchmark study. *IEEE Trans. Pattern Anal. Mach. Intell*. **30**, 2023–2039. (doi:10.1109/TPAMI.2007.70841)
31. Gower JC. 1975 Generalized Procrustes analysis. *Psychometrika* **40**, 33–51. (doi:10.1007/BF02291478)
32. Ten Berge JMF. 1977 Orthogonal Procrustes rotation for two or more matrices. *Psychometrika* **42**, 267–276. (doi:10.1007/BF02294053)
33. Vandeginste BGM, Massart DL, Buydens LMC, Jong S, Lewi PJ, Smeyers-Verbeke J. 1998 Relations between measurement tables. *Data Handl. Sci. Technol.* **20**, 307–347. (doi:10.1016/S0922-3487(98)80045-2)
34. Bieging ET, McGann CJ, Morris A, Rassa A, Cates J. 2014 Left atrial spherical shape change in atrial fibrillation. *J. Cardiovasc. Magn. Reson*. **16**, O41. (doi:10.1186/1532-429X-16-S1-O41)
35. Cates J, Fletcher T, Whitaker R. 2008 A hypothesis testing framework for high-dimensional shape models. In *Proc. 2nd MICCAI Workshop on Mathematical Foundations of Computational Anatomy*, New York, NY, pp. 170–181.
36. Greenacre M, Groenen PJF, Hastie T, D'Enza AI, Markos A, Tuzhilina E. 2022 Principal component analysis. *Nat. Rev. Methods Prim.* **2**, 100. (doi:10.1038/s43586-022-00184-w)
37. Jolliffe IT, Cadima J. 2016 Principal component analysis: a review and recent developments. *Phil. Trans. R. Soc. A.* **374**, 20150202. (doi:10.1098/rsta.2015.0202)
38. Glorfeld LW. 1995 An improvement on Horn's parallel analysis methodology for selecting the correct number of factors to retain. *Educ. Psychol. Meas.* **55**, 377–393. (doi:10.1177/0013164495055003002)
39. Davies RH. 2002 Learning shape: optimal models for analysing natural variability. PhD thesis, University of Manchester, UK.
40. Bieging ET, Morris A, Chang L, Dagher L, Marrouche NF, Cates J. 2021 Statistical shape analysis of the left atrial appendage predicts stroke in atrial fibrillation. *Int. J. Cardiovasc. Imaging* **37**, 2521–2527. (doi:10.1007/s10554-021-02262-8)
41. Nagel C, Luongo G, Azzolin L, Schuler S, Dössel O, Loewe A. 2021 Non-invasive and quantitative estimation of left atrial fibrosis based on P waves of the 12-lead ECG—a large-scale computational study covering anatomical variability. *J. Clin. Med*. **10**, 1797. (doi:10.3390/jcm10081797)
42. Jia S, Nivet H, Harrison J, Pennec X, Camaioni C, Jaïs P, Cochet H, Sermesant M. 2021 Left atrial shape is independent predictor of arrhythmia recurrence after catheter ablation for atrial fibrillation: a shape statistics study. *Heart Rhythm O2* **2**, 622–632. (doi:10.1016/j.hroo.2021.10.013)
43. Bhalodia R, Subramanian A, Morris A, Cates J, Kholmovski E, Marrouche N, Elhabian S. 2019 Does alignment in statistical shape modeling of left atrium appendage impact stroke prediction? In *2019 Computing in Cardiology Conf.*, pp. 1–4. (doi:10.22489/CinC.2019.200)
44. Bieging ET, Morris A, Wilson BD, McGann CJ, Marrouche NF, Cates J. 2018 Left atrial shape predicts recurrence after atrial fibrillation catheter ablation. *J. Cardiovasc. Electrophysiol.* **29**, 966–972. (doi:10.1111/jce.13641)
45. Higuchi K, Cates J, Gardner G, Morris A, Burgon NS, Akoum N, Marrouche NF. 2018 The spatial distribution of late gadolinium enhancement of left atrial magnetic resonance imaging in patients with atrial fibrillation. *JACC Clin. Electrophysiol.* **4**, 49–58. (doi:10.1016/j.jacep.2017.07.016)
46. Varela M, Bisbal F, Zacur E, Berruezo A, Aslanidi OV, Mont L, Lamata P. 2017 Novel computational analysis of left atrial anatomy improves prediction of atrial fibrillation recurrence after ablation. *Front. Physiol.* **8**, 68. (doi:10.3389/fphys.2017.00068)
47. Bademci MS, Ocakoglu G, Kocaaslan C, Bayraktar FA, Tayfur K, Aydin E. 2021 Retrosternal deformations after coronary artery bypass surgery using statistical shape analysis. *Braz. J. Cardiovasc. Surg.* **36**, 670–676. (doi:10.21470/1678-9741-2020-0294)
48. Medrano-Gracia P *et al*. 2014 Left ventricular shape variation in asymptomatic populations: the multi-ethnic study of atherosclerosis. *J. Cardiovasc. Magn. Reson.* **16**, 56. (doi:10.1186/s12968-014-0056-2)
49. Goubergrits L *et al*. 2022 CT-based analysis of left ventricular hemodynamics using statistical shape modeling and computational fluid dynamics. *Front. Cardiovasc. Med.* **9**, 901902. (doi:10.3389/fcvm.2022.901902)
50. Zhang X *et al*. 2014 Atlas-based quantification of cardiac remodeling due to myocardial infarction. *PLoS One* **9**, e110243. (doi:10.1371/journal.pone.0110243)
51. Asif A *et al*. 2023 Assessment of post-infarct ventricular septal defects through 3D printing and statistical shape analysis. *J. 3D Print. Med.* **7**, 3DP3. (doi:10.2217/3dp-2022-0012)
52. Hermida U *et al*. 2023 Left ventricular anatomy in obstructive hypertrophic cardiomyopathy: beyond basal septal hypertrophy. *Eur. Heart J. Cardiovasc. Imaging* **24**, 807–818. (doi:10.1093/ehjci/jeac233)
53. Bernardino G *et al*. 2020 Three-dimensional regional bi-ventricular shape remodeling is associated with exercise capacity in endurance athletes. *Eur. J. Appl. Physiol*. **120**, 1227–1235. (doi:10.1007/s00421-020-04335-3)
54. Pontecorboli G, Biglino G, Milano EG, Sophocleous F, Biffi B, Dastidar AG, Schievano S, Di Mario C, Bucciarelli-Ducci C. 2019 Beyond apical ballooning: computational modelling reveals morphological features of Takotsubo cardiomyopathy. *Comput. Methods Biomech. Biomed. Eng*. **22**, 1103–1106. (doi:10.1080/10255842.2019.1632836)
55. Nam HH *et al*. 2022 Dynamic annular modeling of the unrepaired complete atrioventricular canal annulus. *Ann. Thorac. Surg.* **113**, 654–662. (doi:10.1016/j.athoracsur.2020.12.013)
56. Hermida U *et al*. 2023 Learning the hidden signature of fetal arch anatomy: a three-dimensional shape analysis in suspected coarctation of the aorta. *J. Cardiovasc. Transl. Res.* **16**, 738–747. (doi:10.1007/s12265-022-10335-9)
57. Ardakani VG, Goordoyal H, Ordonez MV, Sophocleous F, Curtis S, Bedair R, Caputo M, Gambaruto A, Biglino G. 2022 Isolating the effect of arch architecture on aortic hemodynamics late after coarctation repair: a computational study. *Front. Cardiovasc. Med.* **9**, 855118. (doi:10.3389/fcvm.2022.855118)
58. Sophocleous F *et al*. 2022 Analysing functional implications of differences in left ventricular morphology using statistical shape modelling. *Sci. Rep.* **12**, 19163. (doi:10.1038/s41598-022-15888-y)
59. Wong J *et al*. 2017 Right ventricular morphology and function following stage I palliation with a modified Blalock–Taussig shunt versus a right ventricle-to-pulmonary artery conduit. *Eur. J. Cardiothorac. Surg.* **51**, 50–57. (doi:10.1093/ejcts/ezw227)
60. Bruse JL *et al*. 2017 Looks do matter! Aortic arch shape after hypoplastic left heart syndrome palliation correlates with cavopulmonary outcomes. *Ann. Thorac. Surg.* **103**, 645–654. (doi:10.1016/j.athoracsur.2016.06.041)

61. Kollar S, Balaras E, Olivieri LJ, Loke YH, Capuano F. 2022 Statistical shape modeling reveals the link between right ventricular shape, hemodynamic force, and myocardial function in patients with repaired tetralogy of Fallot. *Am. J. Physiol. Heart Circ. Physiol*. **323**, H449–H460. (doi:10.1152/ajpheart.00228.2022)
62. Louvelle L, Doyle M, Van Arsdell G, Amon C. 2021 The effect of geometric and hemodynamic parameters on blood flow efficiency in repaired Tetralogy of Fallot patients. *Ann. Biomed. Eng.* **49**, 2297–2310. (doi:10.1007/s10439-021-02771-6)
63. Leonardi B, Taylor AM, Mansi T, Voigt I, Sermesant M, Pennec X, Ayache N, Boudjemline Y, Pongiglione G. 2013 Computational modelling of the right ventricle in repaired tetralogy of Fallot: can it provide insight into patient treatment? *Eur. Heart J. Cardiovasc. Imaging* **14**, 381–386. (doi:10.1093/ehjci/jes239)
64. Narayan HK *et al*. 2020 Atlas-based measures of left ventricular shape may improve characterization of adverse remodeling in anthracycline-exposed childhood cancer survivors: a cross-sectional imaging study. *Cardio Oncol*. **6**, 13. (doi:10.1186/s40959-020-00069-5)
65. Warriner DR *et al*. 2018 An asymmetric wall-thickening pattern predicts response to cardiac resynchronization therapy. *JACC Cardiovasc. Imaging* **11**, 1545–1546. (doi:10.1016/j.jcmg.2018.01.022)
66. Asheghan MM *et al*. 2023 Predicting one-year left ventricular mass index regression following transcatheter aortic valve replacement in patients with severe aortic stenosis: a new era is coming. *Front. Cardiovasc. Med*. **10**, 1130152. (doi:10.3389/fcvm.2023.1130152)
67. Verstraeten S, Hoeijmakers M, Tonino P, Brüning J, Capelli C, van de Vosse F, Huberts W. 2024 Generation of synthetic aortic valve stenosis geometries for in silico trials. *Int. J. Numer. Methods Biomed. Eng*. **40**, e3778. (doi:10.1002/cnm.3778)
68. Cutugno S, Ingrassia T, Nigrelli V, Pasta S. 2021 On the left ventricular remodeling of patients with stenotic aortic valve: a statistical shape analysis. *Bioengineering (Basel)*. **8**, 66. (doi:10.3390/bioengineering8050066)
69. Bosmans B, Huysmans T, Wirix-Speetjens R, Verschueren P, Sijbers J, Bosmans J, Vander Sloten J. 2013 Statistical shape modeling and population analysis of the aortic root of TAVI patients. *J. Med. Device.* **7**, FMD2013–16153. (doi:10.1115/1.4025904)
70. Lopes P, Van Herck PL, Ooms JF, Van Mieghem NM, Wirix-Speetjens R, Sijbers J, Vander Sloten J, Bosmans J. 2022 Automated mitral valve assessment for transcatheter mitral valve replacement planning. *Front. Bioeng. Biotechnol.* **10**, 1033713. (doi:10.3389/fbioe.2022.1033713)
71. Orkild BA *et al*. 2022 All roads lead to Rome: diverse etiologies of tricuspid regurgitation create a predictable constellation of right ventricular shape changes. *Front. Physiol.* **13**, 908552. (doi:10.3389/fphys.2022.908552)
72. Xu J, Desmond EL, Wong TC, Neill CG, Simon MA, Brigham JC. 2022 Right ventricular shape feature quantification for evaluation of pulmonary hypertension: feasibility and preliminary associations with clinical outcome submitted for publication. *J. Biomech. Eng.* **144**, 044502. (doi:10.1115/1.4052495)
73. Fonseca CG *et al*. 2011 The Cardiac Atlas Project—an imaging database for computational modeling and statistical atlases of the heart. *Bioinformatics* **27**, 2288–2295. (doi:10.1093/bioinformatics/btr360)
74. Mauger C *et al*. 2019 Right ventricular shape and function: cardiovascular magnetic resonance reference morphology and biventricular risk factor morphometrics in UK Biobank. *J. Cardiovasc. Magn. Reson.* **21**, 41. (doi:10.1186/s12968-019-0551-6)
75. Bai W, Shi W, de Marvao A, Dawes TJW, O'Regan DP, Cook SA, Rueckert D. 2015 A bi-ventricular cardiac atlas built from 1000+ high resolution MR images of healthy subjects and an analysis of shape and motion. *Med. Image Anal*. **26**, 133–145. (doi:10.1016/j.media.2015.08.009)
76. Hoogendoorn C, Duchateau N, Sánchez-Quintana D, Whitmarsh T, Sukno FM, De Craene M, Lekadir K, Frangi AF. 2013 A high-resolution atlas and statistical model of the human heart from multislice CT. *IEEE Trans. Med. Imaging* **32**, 28–44. (doi:10.1109/TMI.2012.2230015)
77. Ordas S, Oubel E, Leta R, Carreras F, Frangi AF. 2007 A statistical shape model of the heart and its application to model-based segmentation. In *Medical imaging* (eds A Manduca, XP Hu), pp. 490–500. Bellingham, WA: SPIE. (doi:10.1117/12.708879)
78. Rodero C *et al*. 2021 Linking statistical shape models and simulated function in the healthy adult human heart. *PLoS Comput. Biol.* **17**, e1008851. (doi:10.1371/journal.pcbi.1008851)
79. Unberath M, Maier A, Fleischmann D, Hornegger J, Fahrig R. 2015 Open-source 4D statistical shape model of the heart for x-ray projection imaging. In *IEEE 12th Int. Symp. on Biomedical Imaging (ISBI)*, pp. 739–742. IEEE. (doi:10.1109/ISBI.2015.7163978)
80. Nedios S, Tang M, Roser M, Solowjowa N, Gerds-Li JH, Fleck E, Kriatselis C. 2011 Characteristic changes of volume and three-dimensional structure of the left atrium in different forms of atrial fibrillation: predictive value after ablative treatment. *J. Interv. Card. Electrophysiol.* **32**, 87–94. (doi:10.1007/s10840-011-9591-z)
81. Shin SY, Park JW. 2021 Is the left atrial appendage (LAA) anatomical shape really meaningless measure for stroke risk assessment? *Int. J. Cardiol*. **330**, 80–81. (doi:10.1016/j.ijcard.2021.02.047)
82. Farrar G, Suinesiaputra A, Gilbert K, Perry JC, Hegde S, Marsden A, Young AA, Omens JH, McCulloch AD. 2016 Atlas-based ventricular shape analysis for understanding congenital heart disease. *Prog. Pediatr. Cardiol*. **43**, 61–69. (doi:10.1016/j.ppedcard.2016.07.010)
83. Khalafvand SS, Voorneveld JD, Muralidharan A, Gijsen FJH, Bosch JG, van Walsum T, Haak A, de Jong N, Kenjeres S. 2018 Assessment of human left ventricle flow using statistical shape modelling and computational fluid dynamics. *J. Biomech*. **74**, 116–125. (doi:10.1016/j.jbiomech.2018.04.030)
84. Sharp AJ, Pope MT, Briosa e Gala A, Varini R, Banerjee A, Betts TR. 2025 Identifying extra pulmonary vein targets for persistent atrial fibrillation ablation: bridging advanced and conventional mapping techniques. *Europace* **27**, f048. (doi:10.1093/europace/euaf048)
85. Nairn D *et al*. 2023 Differences in atrial substrate localization using late gadolinium enhancement-magnetic resonance imaging, electrogram voltage, and conduction velocity: a cohort study using a consistent anatomical reference frame in patients with persistent atrial fibrillation. *Europace* **25**, euad278. (doi:10.1093/europace/euad278)
86. Azzolin L, Eichenlaub M, Nagel C, Nairn D, Sanchez J, Unger L, Dössel O, Jadidi A, Loewe A. 2023 Personalized ablation vs. conventional ablation strategies to terminate atrial fibrillation and prevent recurrence. *EP Eur*. **25**, 211–222. (doi:10.1093/europace/euac116)
87. Ondrusova B *et al*. 2022 The effect of segmentation variability in forward ECG simulation. In *2022 Computing in Cardiology Conf*, Tampere, Finland, vol. **49**, pp. 1–4, (doi:10.22489/CinC.2022.325)
88. Tate JD, Good WW, Zemzemi N, Boonstra M, van Dam P, Brooks DH, Narayan A, MacLeod RS. 2021 Uncertainty quantification of the effects of segmentation variability in ECGI. In *Lecture notes in computer science functional imaging and modeling of the heart* (eds DB Ennis, LE Perotti, VY Wang), pp. 515–522. Cham, Switzerland: Springer International Publishing. (doi:10.1007/978-3-030-78710-3_49)
89. Medrano-Gracia P, Ormiston J, Webster M, Beier S, Ellis C, Wang C, Smedby Ö, Young A, Cowan B. 2017 A study of coronary bifurcation shape in a normal population. *J. Cardiovasc. Transl. Res.* **10**, 82–90. (doi:10.1007/s12265-016-9720-2)
90. Bruse JL, Giusti G, Baker C, Cervi E, Hsia TY, Taylor AM, Schievano S. 2017 Statistical shape modeling for cavopulmonary assist device development: variability of vascular graft geometry and implications for hemodynamics. *J. Med. Device.* **11**, 021011. (doi:10.1115/1.4035865)
91. Thamsen B *et al*. 2021 Synthetic database of aortic morphometry and hemodynamics: overcoming medical imaging data availability. *IEEE Trans. Med. Imaging* **40**, 1438–1449. (doi:10.1109/TMI.2021.3057496)

92. Kim WJC, Beqiri A, Lewandowski AJ, Mumith A, Sarwar R, King A, Leeson P, Lamata P. 2023 Automated detection of apical foreshortening in echocardiography using statistical shape modelling. *Ultrasound Med. Biol.* **49**, 1996–2005. (doi:10.1016/j.ultrasmedbio.2023.05.003)
93. Zolotarev AM, Khan AKR, Slabaugh G, Roney C. Predicting atrial fibrillation treatment outcome with Siamese multi-modal fusion and cardiac digital twins. In *Proc. of The 7th Int. Conf. on Medical Imaging with Deep Learning (MIDL 2024), Proc. of Machine Learning Research*, vol. **250**, pp. 1927–1938, https://proceedings.mlr.press/v250/zolotarev24a.html.
94. Collins GS, Reitsma JB, Altman DG, Moons KGM. 2014 Transparent reporting of a multivariable prediction model for individual prognosis or diagnosis (TRIPOD): the TRIPOD statement. *BMJ* **350**, g7594–g7594. (doi:10.1136/bmj.g7594)
95. Sheikh M, Fallah SA, Moradi M, Jalali A, Vakili-Basir A, Sahebjam M, Ashraf H, Zoroufian A. 2024 Comparing HeartModelAI and cardiac magnetic resonance imaging for left ventricular volume and function evaluation in patients with dilated cardiomyopathy. *BMC Cardiovasc. Disord.* **24**, 670. (doi:10.1186/s12872-024-04355-3)
96. Herrero-Martín C *et al*. 2025 DYNAMO framework: advancing non-invasive, rapid calibration in cardiac digital twin technology. *Comput. Biol. Med.* **197**, 110974. (doi:10.1016/j.compbiomed.2025.110974)
97. Iyer K, Morris A, Zenger B, Karanth K, Khan N, Orkild BA, Korshak O, Elhabian S. 2022 Statistical shape modeling of multi-organ anatomies with shared boundaries. *Front. Bioeng. Biotechnol.* **10**, 1078800. (doi:10.3389/fbioe.2022.1078800)
98. Cerrolaza JJ, Picazo ML, Humbert L, Sato Y, Rueckert D, Ballester MÁG, Linguraru MG. 2019 Computational anatomy for multi-organ analysis in medical imaging: a review. *Med. Image Anal.* **56**, 44–67. (doi:10.1016/j.media.2019.04.002)
99. Gooya A, Lekadir K, Alba X, Swift AJ, Wild JM, Frangi AF. 2015 Joint clustering and component analysis of correspondenceless point sets: application to cardiac statistical modeling. In *Lecture notes in computer science information processing in medical imaging* (eds G Székely, H Hahn), pp. 98–109. Cham, Switzerland: Springer International Publishing. (doi:10.1007/978-3-319-19992-4_8)
100. Bhalodia R, Elhabian SY, Kavan L, Whitaker RT. 2018 DeepSSM: a deep learning framework for statistical shape modeling from raw images. In *Lecture notes in computer science shape in medical imaging* (eds M Reuter, C Wachinger, H Lombaert, B Paniagua, M Lüthi, B Egger), pp. 244–257. Cham, Switzerland: Springer International Publishing. (doi:10.1007/978-3-030-04747-4_23)
101. Sharp AJ, Betts TR, Banerjee A. 2024 Leveraging 3D atrial geometry for the evaluation of atrial fibrillation: a comprehensive review. *J. Clin. Med.* **13**, 4442. (doi:10.3390/jcm13154442)
102. Adams J, Khan N, Morris A, Elhabian S. 2023 Learning spatiotemporal statistical shape models for non-linear dynamic anatomies. *Front. Bioeng. Biotechnol.* **11**, 1086234. (doi:10.3389/fbioe.2023.1086234)
103. Beetz M *et al*. 2022 Mesh U-Nets for 3D Cardiac Deformation Modeling. In *Statistical Atlases and Computational Models of the Heart. Regular and CMRxMotion Challenge Papers: 13th International Workshop, STACOM 2022*, Held in Conjunction with MICCAI 2022, Singapore, September 18, 2022, Revised Selected Papers, pp. 245–257. Berlin, Heidelberg: Springer-Verlag. (doi:10.1007/978-3-031-23443-9_23)
104. Biffi B, Bruse JL, Zuluaga MA, Ntsinjana HN, Taylor AM, Schievano S. 2017 Investigating cardiac motion patterns using synthetic high-resolution 3D cardiovascular magnetic resonance images and statistical shape analysis. *Front. Pediatr.* **5**, 34. (doi:10.3389/fped.2017.00034)
105. Sophocleous F, Bône A, Shearn AIU, Forte MNV, Bruse JL, Caputo M, Biglino G. 2022 Feasibility of a longitudinal statistical atlas model to study aortic growth in congenital heart disease. *Comput. Biol. Med.* **144**, 105326. (doi:10.1016/j.compbiomed.2022.105326)